Evaluating denoising strategies in resting-state fMRI in traumatic brain injury (EpiBioS4Rx)

Running head title: Denoising fMRI in TBI datasets

Marina Weiler[a*], PhD, Raphael F. Casseb[b*], PhD, Brunno M. de Campos[b], PhD, Julia S. Crone[a], PhD, Evan S. Lutkenhoff[a], PhD, Paul M. Vespa[c], MD, PhD, Martin M. Monti[a,d], PhD, for the EpiBioS4Rx Study Group.

[a] Department of Psychology, University of California Los Angeles, 1285 Franz HallBox 951563, Los Angeles, CA 90095, USA

[b] Neuroimaging Laboratory, University of Campinas, Rua Vital Brasil, 888, Hospital de Clínicas, Cidade Universitária, Campinas, SP, 13083-888, Brazil.

[c] David Geffen School of Medicine, University of California Los Angeles, 10833 Le Conte Ave, Los Angeles, CA 90095, USA

[d] Brain Injury Research Center (BIRC), Department of Neurosurgery, University of California Los Angeles, 300 Stein Plaza Driveway suite 420, Los Angeles, CA 90095, USA

* Co-first authors contributed equally.

Correspondence to:
Martin M. Monti
Department of Psychology
University of California Los Angeles, Los Angeles, CA 90095, USA
monti@psych.ucla.edu

ABSTRACT

Objective: Resting-state functional MRI is increasingly used in the clinical setting and is now included in some diagnostic guidelines for severe brain injury patients. However, to ensure high-quality data, one should mitigate fMRI-related noise typical of this population. Therefore, we aimed to evaluate the ability of different preprocessing strategies to mitigate noise-related signal (*i.e.*, in-scanner movement and physiological noise) in functional connectivity of traumatic brain injury patients.

Methods: We applied nine commonly used denoising strategies, combined into 17 pipelines, to 88 traumatic brain injury patients from the Epilepsy Bioinformatics Study for Anti-epileptogenic Therapy clinical trial (EpiBioS4Rx). Pipelines were evaluated by three quality control metrics across three exclusion regimes based on the participant's head movement profile.

Results: While no pipeline eliminated noise effects on functional connectivity, some pipelines exhibited relatively high effectiveness depending on the exclusion regime. Once high-motion participants were excluded, the choice of denoising pipeline becomes secondary - although this strategy leads to substantial data loss. Pipelines combining spike regression with physiological regressors were the best performers, whereas pipelines that used automated data driven methods performed comparatively worse.

Conclusion: In this study, we report the first large-scale evaluation of denoising pipelines aimed at reducing noise-related functional connectivity in a clinical population known to be highly susceptible to in-scanner motion and significant anatomical abnormalities. If resting-state functional magnetic resonance is to be a successful clinical technique, it is crucial that procedures mitigating the effect of noise be systematically evaluated in the most challenging populations, such as traumatic brain injury datasets.

Keywords: TBI, physiological noise, motion correction, nuisance regression, head motion, artefact.

1. INTRODUCTION

Over the last few decades, the assessment of spontaneous oscillations in the blood oxygenation level-dependent (BOLD) measured by resting-state functional magnetic resonance (rsfMRI) has increasingly been used to aid diagnosis and prognosis in neurological disorders (Baker et al., 2014; de Vos et al., 2018; Franzmeier et al., 2020; Wolters et al., 2019; Woodward et al., 2012). Yet, despite the appeal and wide adoption of this technique, it suffers from significant limitations for distinguishing oscillations associated with neural activity from those induced by non-neural sources (Birn, 2012; Murphy et al., 2013; Power et al., 2017). In-scanner head motion can systematically generate artifactual correlations across brain regions and spurious functional connectivity (FC) results regardless of how they are assessed (e.g., seed-based analysis, graph theory, amplitude of low frequency fluctuations)(Power et al., 2012; Satterthwaite et al., 2012; Van Dijk et al., 2012).

In the context of severe brain injury and disorders of consciousness, some international guidelines (Kondziella et al., 2020) now suggest incorporating rsfMRI in the diagnostic process given its ability to complement bedside neurobehavioral assessments and provide prognostic information (Demertzi et al., 2019; Madhavan et al., 2019; Silva et al., 2015; Vanhaudenhuyse et al., 2010). However, this patient group is well known to exhibit high incidence of in-scanner motion during data acquisitions (Hannawi et al., 2016; Monti et al., 2015), which can corrupt estimates of FC. While this issue could be mitigated with the use of sedative agents, these will affect any subsequent analysis of brain network function (Monti et al., 2013), thus making the development of analytical approaches to mitigating in-scanner motion a more desirable strategy. In this sense, a large number of analysis pipelines have been proposed to address the issue (Muschelli et al., 2014; Power et al., 2015). However, most of this work has been developed and evaluated in neurotypical individuals or clinical populations that do not usually present significant anatomical abnormalities (Burgess et al., 2016; Ciric et al., 2018; Parkes et al., 2018; Power et al., 2020; Raval et al., 2020). No pipeline has ever been validated with respect to patients exhibiting the degree of in-scanner motion (Hannawi et al., 2016; Monti et al., 2015) and the extensive brain pathology (such as atrophy and trauma-induced deformations) known to lead to sub-optimal and biased performance of conventional analysis software (Lutkenhoff et al., 2014). If rsfMRI is to be a successful technique used in routine clinical practice (Kondziella et al., 2020), it is crucial that procedures mitigating the effect of noise be systematically evaluated also in the most challenging populations.

To address this gap, we extend a prior large-scale evaluation of different pipelines (Parkes et al., 2018) to the very challenging population of moderate-to-severe traumatic brain injury (TBI) to provide a

quantitative comparative assessment of different denoising strategies. Specifically, we applied nine commonly used denoising strategies, combined into 17 pipelines, to TBI patients from the Epilepsy Bioinformatics Study for Anti-epileptogenic Therapy clinical trial (EpiBioS4Rx) (Vespa et al., 2019) and evaluated the ability of each one to remove noise from the BOLD signal. We conclude by providing a framework for clinicians and translational scientists interested in using fMRI to select the pipeline that balances the ability to mitigate noise with the constraints and aims of their study.

2. METHODS

2.1 Subjects

This study included 88 patients from the EpiBioS4Rx dataset, a longitudinal study that aims to discover and validate observational biomarkers of epileptogenesis after TBI (Vespa et al., 2019). As described elsewhere, patients were enrolled across 12 sites within 72 hours following TBI involving frontal and/or temporal hemorrhagic contusion, according to criteria previously published (Vespa et al., 2019). Our sample consisted of 21 females and 67 males, with mean age 41.1 (7-84) years, level of consciousness after TBI measured by the Glasgow Coma Scale (Teasdale and Jennett, 1974) 7.8 (1-15), and time since injury 11 (0-36) days. Informed consent was obtained from a surrogate family member or legally authorized representative, using IRB-approved consent methods.

2.2 Image Acquisition and Processing

Data were acquired on 1.5 or 3T MR system, including an anatomical (T1-weighted) and functional (T2*-weighted echo planar images) acquisitions (See **Suppl. Tables 1** and **2** for detailed parameter listing.) Data were processed using code adapted from (Parkes et al., 2018) (https://github.com/lindenmp/rs-fMRI). Before temporal and spatial filtering, preprocessed data were submitted to denoising strategies (see below).

2.3 Denoising Strategies

Denoising is achieved by removing variance attributable to head and respiration/cardiac -induced motion from the BOLD signal. What is debated is how to best measure, operationalize, and remove these sources of noise. **Table 1** summarizes the denoising approaches used in our analysis. We combined these approaches into 17 pipelines, as done in prior work that used a different clinical sample (Parkes et al., 2018).

2.4 Head Movement Estimation (in-scanner motion)

As shown in **Table 1**, some pipelines rely on the ability to pinpoint volumes corrupted by excessive motion. In general, motion in a volume is quantified by the Derivative of the root mean squares VARiance over voxelS (DVARS) (Power et al., 2012; Smyser et al., 2011) and Framewise Displacement (FD) (Jenkinson et al., 2002; Power et al., 2012), which were used here for spike regression and scrubbing approaches. In addition, we calculated in-scanner head movement for each patient, used to calculate quality control measures, and classify each patient under an exclusion regime. For that, we used the mean FD_{Jenk} (Jenkinson et al., 2002) across all volumes (hereafter, mFD).

2.5 Quality Control (QC) Measures

After image preprocessing, we used a template containing 333 cortical regions (ROIs) (Gordon et al., 2016) to define the areas to extract gray matter (GM)-weighed denoised time-series for further analysis. We then calculated FC as Pearson's correlation coefficient between each pair of ROI time-series, then implemented a Fisher's r-to-z transformation. The FC matrices obtained following each denoising pipeline were then used to evaluate the ability of each pipeline to remove noise-induced correlations by the two quality control measures described below.

2.5.1 QC-FC correlation. Represents the correlation between FC and in-scanner head motion (mFD) since non-neuronal fluctuations can increase the apparent FC between regions by introducing spurious common variance across time series. Here, we calculated Pearson's correlation coefficient between each pair of ROIs FC and the mFD across patients.

2.5.2 QC-FC distance-dependence. Indicates whether the correlation between FC and in-scanner head motion (mFD) is spatially structured – a known feature of motion-induced artifacts (Power et al., 2012; Power et al., 2014; Satterthwaite et al., 2012; Van Dijk et al., 2012). Here, we calculated the distance between ROIs as the Euclidean distance between the stereotaxic coordinates of the volumetric centers of ROI pairs. We quantified the relationship between this distance and the QC-FC correlation for each edge using Spearman's rank correlation coefficient (ρ) due to the non-linearity of some associations.

In addition, we measured the ability of each pipeline to retain statistical power during the denoising process:

2.5.3 loss of temporal degrees of freedom (tDOF-loss). Represents the amount of tDOF lost due to the removal of time points and/or to the number of regressors used to denoise the data (**Suppl. Table 3**).

2.6 Participant Exclusion Regimes

Finally, it is debated how to determine the threshold at which a subject contains excessive motion and thus should be discarded from any analysis. We compared the performance of all pipelines under three different participant exclusion regimes: (*i*) censoring-based, (*ii*) lenient, and (*iii*) stringent (**Table 2** shows criteria for subject exclusion in each regime).

3. RESULTS

3.1 Head Movement and Participant Exclusion

As shown in **Fig. 1a**, censoring-based, lenient, and stringent regimes resulted in the exclusion of 8, 11, and 32 patients (9 %, 12.5 %, and 36 %, respectively). As expected, participants under the stringent regime presented significantly smaller mFD compared to censoring-based and lenient regimes (**Fig. 1b**, Kruskal-Wallis test, $H(2) = 9.791$, $p = 0.0075$; mean rank mFD 116.45 for censoring-based, 113.18 for lenient and 85.00 for stringent. Pairwise comparisons Bonferroni-adjusted for multiplicity: stringent vs lenient, $p = 0.028$; stringent vs censoring-based, $p = 0.01$; lenient vs censoring-based, $p = 1$). In-scanner head movement did not correlate with Glasgow Coma Scale (Pearson $r(84) = 0.080$, $p = 0.462$), age (Pearson $r(85) = 0.139$, $p = 0.201$), nor time since injury (Pearson $r(79) = 0.128$, $p = 0.253$). A logistic regression was performed to ascertain the effects of age, gender, time since injury, and Glasgow Coma Scale on the likelihood that participants would fall into the Stringent regime. The logistic regression model was not statistically significant, $\chi2(4) = 6.051$, $p = .195$. The model explained 10% (Nagelkerke R^2) of the variance in Stringent regime and correctly classified 63% of cases.

3.2 Quality Control Measures

As shown in **Fig. 2** and **3**, consistent with prior work (Parkes et al., 2018), while no pipeline entirely eliminated noise-related effects on FC patterns, some pipelines exhibited relatively high effectiveness at mitigating it depending on the exclusion regime.

3.2.1 QC-FC. Overall, no pipeline in any exclusion regime reduced the effect of noise to zero (**Fig. 2**). Nonetheless, our results show that some pipelines, under a given regime, perform better than others.

First, the censoring-based and lenient regimes resulted in approximately 10-29 % and 13-55 % proportion of significant correlations and absolute *r*-values between 0.09-0.14and 0.10-0.24, respectively. 6HMP pipeline was an outlier with ~92 % proportion of QC-FC significant correlations and an absolute correlation between motion and FC of 0.38 in the lenient regime. In comparison, the stringent criterion resulted in lower QF-FC across all pipelines, reducing the correlations significantly

to less than 10 % and median *r*-value between motion and FC to 0.09-0.11 (with the sole exception of the 6HMP, with ~20 % significant correlations).

Second, within each of the three exclusion regimes, different strategies exhibit different effectiveness at mitigating noise. Overall, in the (*i*) censoring-based regime, the best performance was obtained with different combinations of 24HMP, aCompCor, and spike regression. Conversely, the three worst performing pipelines all featured data-driven methods, including aCompCor50 and ICA-AROMA. The addition of GSR generally resulted in the worsening of pipeline performance. Under the (*ii*) lenient regime, a very different pattern of results was observed. Overall, the best performing pipelines under this regime were the two featuring aCompCor, spike regression, and GSR, with either 6 or 24 HMP. At the opposite end of performance, pipelines without GSR underperformed those with GSR, and the pipeline with 6HMP alone resulted in the slightest mitigation of noise-induced effects on FC. The inclusion of GSR improved pipeline performance for all pipelines, with the greatest benefit observed for the aCompCor/aCompCor50 pipelines. Overall, in the (*iii*) stringent regime, the pipelines performed similarly one to another (with the sole exception of the 6HMP), and all pipelines performed better under the stringent regime than censoring-based and lenient regimes, reducing significantly QC-FC correlations. The inclusion of GSR barely changed any pipeline performance under this regime.

3.2.2 QC-FC Distance-Dependence. As shown in **Fig. 3**, the proportion of statistically significant correlations between QC-FC and ROI distance for each denoising pipeline in each regime is comparable to prior validations (Parkes et al., 2018). Like QC-FC, the stringent regime reduced distance dependence on QC-FC the most (with an absolute average correlation of 0.06), followed by the lenient and the censoring-based criteria (absolute average correlation of 0.16 and 0.25, respectively).

Specifically, in the (*i*) censoring-based regime, pairing aCompCor with spike regression resulted in the lowest correlations (*i.e.*, best performance) between distance and QC-FC whether performed together with 6HMP, 24HMP, or GSR. Similarly, 24HMP with 2phys and spike regression also resulted in a low QF-FC distance dependence. Like QC-FC, the three worst pipelines all included data-driven methods (ICA-AROMA with 2phys; ICA-AROMA with 2phys and GSR; and 24HMP with aCompCor50, and GSR). Likewise, scrubbing (with 24HMP, 2phys, with or without GSR) resulted in poor performance under this exclusion regime. Overall, the inclusion of GSR worsened pipeline performance across the board. Under the (*ii*) lenient regime, the combination of aCompCor with spike regression, whether with 6 or 24HMP, resulted in very low correlations (*i.e.*, good performance), only surpassed by the combination of ICA-AROMA with 2phys and 24HMP with 2phys and spike

regression. The addition of GSR also worsened performance across all pipelines under this regime. aCompCor50 (with GSR) was the worst performer, followed by scrubbing paired with 24HMP, 2phys, and GSR, and 24HMP paired with 2phys and GSR. Finally, under the (*iii*) stringent regime, the combination of aCompCor and spike regression, whether with 6 or 24HMP, resulted in the lowest correlations (*i.e.*, best performance). The addition of GSR generally resulted in unchanged or worse performance, with 24HMP with aCompCor50 and GSR resulting in the most significant absolute correlation.

3.2.3 tDOF-Loss. As expected, the stringent regime resulted in the lowest average loss of tDOF (since the high-movement subjects were excluded), albeit at the detriment of group degrees of freedom – given the large loss of sample size. Scrubbing resulted in the most significant tDOF-loss across all regimes (**Fig. 4**).

4. DISCUSSION

In this study, we report the first large-scale evaluation of denoising pipelines aimed at reducing noise-related FC in a clinical population known to be highly susceptible to in-scanner motion (Hannawi et al., 2016; Monti et al., 2015) and to present considerable anatomical abnormalities. Overall, we report three main findings.

First, one of the most critical aspects of successful denoising is selecting which subjects to retain for further analysis (Satterthwaite et al., 2013; Satterthwaite et al., 2012; Van Dijk et al., 2012). In this high-motion cohort, a stringent selection obviously resulted in equal or better performance in QC metrics across virtually all pipelines. In other words, once high-motion participants are removed from the sample, the choice of denoising pipeline becomes secondary (with the sole exception of the 6HMP approach). Nonetheless, while the quality of the data used for analysis benefits significantly from this approach, it is very costly in terms of data loss (37% in our sample). Consequently, it decreases the degrees of freedom for statistical inference across groups (such as performing group comparison between patients and volunteers or correlation analysis between behavioral scores on a test of interest and FC metrics).

Second, different denoising approaches exhibit very distinct abilities to mitigate the negative effects of noise on FC (Parkes et al., 2018). Pipelines combining spike regression with 2phys and its extension, aCompCor, tend to be the best performers across exclusion regimes. Somewhat unexpectedly, pipelines using scrubbing, ICA-AROMA, and aCompCor50 performed comparatively worse. Overall, pipelines using scrubbing were generally either comparable or worse than the other ones, in addition to the cost

of two to three times greater loss of tDOF—up to 50% of the available data per subject—thus hampering the quality of the FC estimates. Pipelines containing data-driven techniques (*i.e.*, ICA-AROMA and aCompCor50), which can be very effective at removing noise-related artifacts (Pruim et al., 2015), were instead among the worst performers under most regimes. While it is hard to pinpoint the source of their poor performance, we could speculate that the structural features of our images pose too great an obstacle to be addressed by these denoising approaches. aCompCor50 and ICA-AROMA, for example, rely on the accurate segmentation of brain tissues to identify noise components. TBI patients constitute a very heterogeneous sample from which segmenting the brain into different tissues might be challenging, probably affecting the performance of denoising strategies that depend on this step. Indeed, ICA-AROMA at times could not find any "signal" components in some patients (*i.e.*, all components were classified as noise, **Suppl. Fig1**), stressing that these methods should be used with care when dealing with datasets containing pathological brains (Heine et al., 2012).

Third, we find the addition of GSR, a controversial step in fMRI data preprocessing, to give mixed results. On the one hand, it did improve the QC-FC metric under the lenient and stringent regimes (albeit only very marginally in the latter). On the other hand, it worsened the distance-dependent QC metric for virtually all pipelines, under all regimes—consistent with prior reports (Ciric et al., 2017).

Given these results, we offer three recommendations. First, where possible, use a stringent exclusion regime. This approach essentially reduces the analyzed sample to low-motion subjects, thus ensuring that systematic spurious correlations do not affect FC estimates. While the data loss can be sizeable (37% in our sample), this approach leads to the most significant mitigation of the negative effects of noise on FC. In addition, this strategy also gives the researcher freedom to choose among almost any pipeline, according to which procedure is best for the study's goals. However, this approach has the potential for biased data loss. For example, some patients might be more motion-prone, resulting in greater exclusion rates and thus hampering group analyses.

Second, when choosing between pipelines, we find combinations of 2phys, spike regression and aCompCor to perform best in general. Scrubbing, in turn, performed relatively poorly under most circumstances and led to a high loss in tDOF. Likewise, ICA-AROMA—which has been shown to perform very well in healthy volunteers (Pruim et al., 2015)—underperformed many pipelines in our clinical sample. While the reason why this approach was not very effective remains unsolved, we speculate that the segmentation of tissue compartments can be very problematic in the presence of significant brain shape deformation (*e.g.*, due to primary impact damage, ventricular enlargement,

among others). Finally, given the mixed results and the controversial nature of this step, we do not recommend using GSR.

There are several limitations to the current work that should be acknowledged. First, our results are limited to the combination of approaches we chose for each pipeline. While some pipelines outperformed others, we should bear in mind that different combinations could yield divergent results (*e.g.*, adding quadratic and derivative terms of physiological or global signal). Likewise, our results reflect the performance of pipelines for our particular image acquisition parameters. Testing these pipelines in images with shorter or longer TRs and other parameters should be addressed in future work. Second, the participants excluded from censoring pipelines (*i.e.*, participants with < 4 min of data based on spike regression or scrubbing) were also excluded from the other pipelines. While we thought it was crucial to compare pipelines maintaining the number of subjects constant across them, it also precluded us from evaluating how non-censoring pipelines would perform without this criterion. Future work should focus on assessing, for example, how data-driven approaches perform when including these participants. Lastly, our QC measures focused on a specific way of calculating FC (*i.e.*, a model-based method using Pearson's correlation between ROIs time series). We recognize that other metrics of FC (see (Li et al., 2009)) could result in different findings.

Taken together, our findings stress the heterogeneous performance of denoising pipelines, emphasizing that different strategies may be appropriate in the context of specific goals, according to the question and study design. Researchers should be familiar with their samples regarding head movement profile and clinical features and be aware of each approach's strengths and weaknesses to find the pipeline that best matches their goals.

5. AUTHOR CONTRIBUTIONS

The authors confirm contribution to the paper as follows: MW, RFC and MMM conceived and designed the study; the Epilepsy Bioinformatics Study for Anti-epileptogenic Therapy clinical trial (EpiBioS4Rx) research group (**Suppl. Table 4**) collected the data; MW, RFC, BMC, JSC, ESL, PMV and MMM contributed with analysis tools; MW and RFC performed the analysis; MW, RFC, BMC, JSC, ESL, PMV and MMM wrote the paper.

6. CONFLICT OF INTEREST

The authors declare that there is no conflict of interest.

7. FUNDING

This work was supported by the National Institute of Neurological Disorders and Stroke (NINDS) U54 NS100064 (EpiBioS4Rx), FAPESP (São Paulo Research Foundation) #2020/00019-7 and #2013/07559-3, Tiny Blue Dot Foundation, Interuniversity Cluster Project University of Vienna - FWF Austrian Science Fund Connecting Minds #CMW 30-B, and NIH Pathway to Independence 1K99NS104243-01.

8. REFERENCES

Baker, J.T., Holmes, A.J., Masters, G.A., Yeo, B.T.T., Krienen, F., Buckner, R.L., Ongur, D., 2014. Disruption of Cortical Association Networks in Schizophrenia and Psychotic Bipolar Disorder. Jama Psychiatry 71, 109-118.
Birn, R.M., 2012. The role of physiological noise in resting-state functional connectivity. Neuroimage 62, 864-870.
Burgess, G.C., Kandala, S., Nolan, D., Laumann, T.O., Power, J.D., Adeyemo, B., Harms, M.P., Petersen, S.E., Barch, D.M., 2016. Evaluation of Denoising Strategies to Address Motion-Correlated Artifacts in Resting-State Functional Magnetic Resonance Imaging Data from the Human Connectome Project. Brain Connect 6, 669-680.
Ciric, R., Rosen, A.F.G., Erus, G., Cieslak, M., Adebimpe, A., Cook, P.A., Bassett, D.S., Davatzikos, C., Wolf, D.H., Satterthwaite, T.D., 2018. Mitigating head motion artifact in functional connectivity MRI. Nat Protoc 13, 2801-2826.
Ciric, R., Wolf, D.H., Power, J.D., Roalf, D.R., Baum, G.L., Ruparel, K., Shinohara, R.T., Elliott, M.A., Eickhoff, S.B., Davatzikos, C., Gur, R.C., Gur, R.E., Bassett, D.S., Satterthwaite, T.D., 2017. Benchmarking of participant-level confound regression strategies for the control of motion artifact in studies of functional connectivity. Neuroimage 154, 174-187.
de Vos, F., Koini, M., Schouten, T.M., Seiler, S., van der Grond, J., Lechner, A., Schmidt, R., de Rooij, M., Rombouts, S., 2018. A comprehensive analysis of resting state fMRI measures to classify individual patients with Alzheimer's disease. Neuroimage 167, 62-72.
Demertzi, A., Tagliazucchi, E., Dehaene, S., Deco, G., Barttfeld, P., Raimondo, F., Martial, C., Fernandez-Espejo, D., Rohaut, B., Voss, H.U., Schiff, N.D., Owen, A.M., Laureys, S., Naccache, L., Sitt, J.D., 2019. Human consciousness is supported by dynamic complex patterns of brain signal coordination. Science Advances 5, eaat7603.
Franzmeier, N., Neitzel, J., Rubinski, A., Smith, R., Strandberg, O., Ossenkoppele, R., Hansson, O., Ewers, M., Adni, 2020. Functional brain architecture is associated with the rate of tau accumulation in Alzheimer's disease. Nature Communications 11.
Gordon, E.M., Laumann, T.O., Adeyemo, B., Huckins, J.F., Kelley, W.M., Petersen, S.E., 2016. Generation and Evaluation of a Cortical Area Parcellation from Resting-State Correlations. Cereb Cortex 26, 288-303.
Hannawi, Y., Abers, M.S., Geocadin, R.G., Mirski, M.A., 2016. Abnormal movements in critical care patients with brain injury: a diagnostic approach. Critical care (London, England) 20, 60-60.
Heine, L., Soddu, A., Gomez, F., Vanhaudenhuyse, A., Tshibanda, L., Thonnard, M., Charland-Verville, V., Kirsch, M., Laureys, S., Demertzi, A., 2012. Resting State Networks and Consciousness. Frontiers in Psychology 3.
Jenkinson, M., Bannister, P., Brady, M., Smith, S., 2002. Improved Optimization for the Robust and Accurate Linear Registration and Motion Correction of Brain Images. Neuroimage 17, 825-841.

Kondziella, D., Bender, A., Diserens, K., van Erp, W., Estraneo, A., Formisano, R., Laureys, S., Naccache, L., Ozturk, S., Rohaut, B., Sitt, J.D., Stender, J., Tiainen, M., Rossetti, A.O., Gosseries, O., Chatelle, C., Ean Panel on Coma, D.o.C., 2020. European Academy of Neurology guideline on the diagnosis of coma and other disorders of consciousness. European Journal of Neurology 27, 741-756.

Li, K., Guo, L., Nie, J., Li, G., Liu, T., 2009. Review of methods for functional brain connectivity detection using fMRI. Computerized medical imaging and graphics : the official journal of the Computerized Medical Imaging Society 33, 131-139.

Lutkenhoff, E.S., Rosenberg, M., Chiang, J., Zhang, K., Pickard, J.D., Owen, A.M., Monti, M.M., 2014. Optimized brain extraction for pathological brains (optiBET). PloS One 9, e115551.

Madhavan, R., Joel, S.E., Mullick, R., Cogsil, T., Niogi, S.N., Tsiouris, A.J., Mukherjee, P., Masdeu, J.C., Marinelli, L., Shetty, T., 2019. Longitudinal Resting State Functional Connectivity Predicts Clinical Outcome in Mild Traumatic Brain Injury. J Neurotrauma 36, 650-660.

Monti, M.M., Lutkenhoff, E.S., Rubinov, M., Boveroux, P., Vanhaudenhuyse, A., Gosseries, O., Bruno, M.A., Noirhomme, Q., Boly, M., Laureys, S., 2013. Dynamic change of global and local information processing in propofol-induced loss and recovery of consciousness. PLoS Comput Biol 9, e1003271.

Monti, M.M., Rosenberg, M., Finoia, P., Kamau, E., Pickard, J.D., Owen, A.M., 2015. Thalamo-frontal connectivity mediates top-down cognitive functions in disorders of consciousness. Neurology 84, 167-173.

Murphy, K., Birn, R.M., Bandettini, P.A., 2013. Resting-state fMRI confounds and cleanup. Neuroimage 80, 349-359.

Muschelli, J., Nebel, M.B., Caffo, B.S., Barber, A.D., Pekar, J.J., Mostofsky, S.H., 2014. Reduction of motion-related artifacts in resting state fMRI using aCompCor. Neuroimage 96, 22-35.

Parkes, L., Fulcher, B., Yücel, M., Fornito, A., 2018. An evaluation of the efficacy, reliability, and sensitivity of motion correction strategies for resting-state functional MRI. Neuroimage 171, 415-436.

Power, J.D., Barnes, K.A., Snyder, A.Z., Schlaggar, B.L., Petersen, S.E., 2012. Spurious but systematic correlations in functional connectivity MRI networks arise from subject motion. Neuroimage 59, 2142-2154.

Power, J.D., Lynch, C.J., Adeyemo, B., Petersen, S.E., 2020. A Critical, Event-Related Appraisal of Denoising in Resting-State fMRI Studies. Cerebral Cortex 30, 5544-5559.

Power, J.D., Mitra, A., Laumann, T.O., Snyder, A.Z., Schlaggar, B.L., Petersen, S.E., 2014. Methods to detect, characterize, and remove motion artifact in resting state fMRI. Neuroimage 84, 320-341.

Power, J.D., Plitt, M., Laumann, T.O., Martin, A., 2017. Sources and implications of whole-brain fMRI signals in humans. Neuroimage 146, 609-625.

Power, J.D., Schlaggar, B.L., Petersen, S.E., 2015. Recent progress and outstanding issues in motion correction in resting state fMRI. Neuroimage 105, 536-551.

Pruim, R.H.R., Mennes, M., Buitelaar, J.K., Beckmann, C.F., 2015. Evaluation of ICA-AROMA and alternative strategies for motion artifact removal in resting state fMRI. Neuroimage 112, 278-287.

Raval, V., Nguyen, K.P., Mellema, C., Montillo, A., 2020. Improved motion correction for functional MRI using an omnibus regression model. Proc IEEE Int Symp Biomed Imaging 2020, 1044-1047.

Satterthwaite, T.D., Elliott, M.A., Gerraty, R.T., Ruparel, K., Loughead, J., Calkins, M.E., Eickhoff, S.B., Hakonarson, H., Gur, R.C., Gur, R.E., Wolf, D.H., 2013. An improved framework for confound regression and filtering for control of motion artifact in the preprocessing of resting-state functional connectivity data. Neuroimage 64, 240-256.

Satterthwaite, T.D., Wolf, D.H., Loughead, J., Ruparel, K., Elliott, M.A., Hakonarson, H., Gur, R.C., Gur, R.E., 2012. Impact of in-scanner head motion on multiple measures of functional connectivity: relevance for studies of neurodevelopment in youth. Neuroimage 60, 623-632.

Silva, S., de Pasquale, F., Vuillaume, C., Riu, B., Loubinoux, I., Geeraerts, T., Seguin, T., Bounes, V., Fourcade, O., Demonet, J.F., Péran, P., 2015. Disruption of posteromedial large-scale neural communication predicts recovery from coma. Neurology 85, 2036-2044.

Smyser, C.D., Snyder, A.Z., Neil, J.J., 2011. Functional connectivity MRI in infants: exploration of the functional organization of the developing brain. Neuroimage 56, 1437-1452.

Teasdale, G., Jennett, B., 1974. Assessment of coma and impaired consciousness. A practical scale. Lancet 2, 81-84.
Van Dijk, K.R., Sabuncu, M.R., Buckner, R.L., 2012. The influence of head motion on intrinsic functional connectivity MRI. Neuroimage 59, 431-438.
Vanhaudenhuyse, A., Noirhomme, Q., Tshibanda, L.J., Bruno, M.A., Boveroux, P., Schnakers, C., Soddu, A., Perlbarg, V., Ledoux, D., Brichant, J.F., Moonen, G., Maquet, P., Greicius, M.D., Laureys, S., Boly, M., 2010. Default network connectivity reflects the level of consciousness in non-communicative brain-damaged patients. Brain 133, 161-171.
Vespa, P.M., Shrestha, V., Abend, N., Agoston, D., Au, A., Bell, M.J., Bleck, T.P., Blanco, M.B., Claassen, J., Diaz-Arrastia, R., Duncan, D., Ellingson, B., Foreman, B., Gilmore, E.J., Hirsch, L., Hunn, M., Kamnaksh, A., McArthur, D., Morokoff, A., O'Brien, T., O'Phelan, K., Robertson, C.L., Rosenthal, E., Staba, R., Toga, A., Willyerd, F.A., Zimmermann, L., Yam, E., Martinez, S., Real, C., Engel, J., Jr., 2019. The epilepsy bioinformatics study for anti-epileptogenic therapy (EpiBioS4Rx) clinical biomarker: Study design and protocol. Neurobiol Dis 123, 110-114.
Wolters, A.F., van de Weijer, S.C.F., Leentjens, A.F.G., Duits, A.A., Jacobs, H.I.L., Kuijf, M.L., 2019. "Resting-state fMRI in Parkinson's disease patients with cognitive impairment: A meta-analysis": Answer to Wang and colleagues. Parkinsonism & Related Disorders 66, 253-254.
Woodward, N.D., Karbasforoushan, H., Heckers, S., 2012. Thalamocortical Dysconnectivity in Schizophrenia. American Journal of Psychiatry 169, 1092-1099.

FIGURE LEGENDS

Fig1: (a) Number of participants excluded in each regime; (b) Box plots of the mFD values for each regime.

Fig2: QC-FC correlations under the three regimes of participant exclusion. On the left of each panel, results are shown as the proportion of significant FCs that correlated with the patient's head movement (mFD), $p < 0.05$. On the right of each panel, results are shown as the full distribution of QC-FC, and the corresponding median value. Better denoising pipelines result in fewer correlations between FC and head movement, giving values closer to 0.

Fig3: QC-FC distance-dependence under the three participant exclusion regimes. Results are presented as Spearman's ρ correlation coefficient. Better denoising pipelines result in fewer correlations between FC and head movement, giving values closer to 0.

Fig4: Temporal degrees of freedom loss (tDOF-loss) under the three regimes of participant exclusion. Results are presented as mean ± standard deviation. Ideally, good denoising pipelines should use fewer regressors in the model, losing fewer degrees of freedom and resulting in values closer to 0.

Suppl. Fig1: Box plot showing the percentage of components classified as noise by ICA-AROMA for each patient. When 100, it means that all components were classified as noise by the classifier.

Table 1: Denoising strategies.

Head displacement	**Head Motion Parameters (HMP)**: Six parameters (3 rotations and 3 translations about/along the X-, Y-, and Z-axes) included as noise regressors (6HMP)[36]. Additional regressors derived from the six parameters (*e.g.*, temporal and quadratic terms of each parameter, as well as their difference) are often included to account for delayed and nonlinear motion-induced spin history effects (24HMP)[31]. **Spike Regression**[31]: For each volume containing excessive motion, a separate regressor is generated containing a value of 1 at that volume, and 0 at all others. Volumes are considered contaminated if FD_{Jenk}[28] > 0.25 mm. FD_{Jenk} represents the root mean squared of the 6 motion parameters[28]. **Scrubbing**[29]: Each volume containing excessive motion is removed from the time-series if FD_{Power}[9] > 0.2 mm or DVARS[9,27] > 2 %. After removal, uncontaminated segments of BOLD data lasting fewer than 5 contiguous volumes are also removed. FD_{Power} represents the sum of the absolute values of the differentiated realignment estimates (by backward differences) at every time-point[9].
Physiology-related	**Physiological Regressors (2phys)**: Regression of the average signal from WM and CSF, tissues not expected to exhibit BOLD oscillations tied to neural activity. **Anatomical Component Based Correction (aCompCor[37]/aCompCor50[38])**: This approach involves extracting orthogonal components of temporal variance from voxel-wise time series for the WM and CSF masks separately. Then, either the five components with greater eigenvalue for each tissue are included in the denoising regression (aCompCor), or as many components as needed to cumulatively explain at least 50% of the variance in each tissue (aCompCor50).
Mixed approaches	**Global Signal Regression (GSR)**: Regression of the average signal across all the voxels of the brain. **ICA-based Automatic Removal Of Motion Artifacts (ICA-AROMA[39])**: Automated data-driven method to identify and remove via regression motion-related independent components.

Abbreviations: FD = framewise displacement; DVARS = derivative of the root mean squares variance over voxels; BOLD = blood oxygenation level-dependent; WM = white matter; CSF = cerebrospinal fluid; ICA = independent component analysis.

Table 2: Participant exclusion regimes and their criteria for exclusion:

Regime	Exclusion criteria
Censoring-based(Satterthwaite et al., 2013; Van Dijk et al., 2012)	Excluded subjects when less than 4 minutes of non-contaminated volumes remained after volume censoring (< 4 minutes of data).
Lenient(Satterthwaite et al., 2012)	Excluded subjects if: (i) < 4 minutes of data; or (ii) high levels of head gross motion, defined as mFD > 0.55mm.
Stringent(Satterthwaite et al., 2013)	Excluded subjects if: (i) < 4 minutes of data; (ii) mFD > 0.25 mm; (iii) more than 20% of the volumes presented FD_{Jenk} > 0.2 mm; or (iv) any volume presented FD_{Jenk} > 5mm.

Abbreviations: FD = framewise displacement; mFD = mean framewise displacement.

Suppl. Table 1: Detailed T1 image acquisition parameters:

Subj	Mag Field	Software	Model	Matrix		Voxel Size		Slice Thickness	Slices	TR (ms)	TE (ms)	Flip Angle
1	3T	SIEMENS	Skyra	256	256	1	1	1	256	2300	2.26	8
2	3T	SIEMENS	Skyra	256	256	1	1	1	256	2300	2.26	8
3	3T	SIEMENS	Skyra	256	256	1	1	1	256	2300	2.26	8
4	3T	SIEMENS	Skyra	256	256	1	1	1	256	2300	2.26	8
5	3T	SIEMENS	Skyra	256	256	1	1	1	256	2300	2.26	8
6	3T	SIEMENS	Skyra	256	256	1	1	1	256	2300	2.26	8
7	3T	SIEMENS	Skyra	256	256	1	1	1	256	2300	2.26	8
8	3T	SIEMENS	Skyra	256	256	1	1	1	256	2300	2.26	8
9	3T	SIEMENS	Skyra	256	256	1	1	1	256	2300	2.26	8
10	3T	SIEMENS	Skyra	256	256	1	1	1	256	2300	2.26	8
11	3T	SIEMENS	Skyra	256	256	1	1	1	256	2300	2.26	8
12	3T	Philips	Ingenia	256	256	1	1	1	256	8.196	3.753	8
13	3T	Philips	Ingenia	256	256	1	1	1	256	8.247	3.776	8
14	3T	Philips	Ingenia	256	256	1	1	1	256	8.142	3.721	8
15	3T	Philips	Ingenia	280	220	0.49	0.49	0.9	512	9.01	4.124	8
16	3T	Philips	Ingenia	256	256	1	1	1	256	8.233	3.771	8
17	3T	Philips	Ingenia	256	256	1	1	1	256	8.397	3.86	8
18	3T	GE	Signa	256	256	1	1	1	256	8.856	3.488	15
19	3T	GE	Signa	256	256	1	1	1	256	9.088	3.624	15
20	3T	GE	Signa	256	256	1	1	1	256	8.824	3.488	15
21	3T	GE	Signa	256	256	1	1	1	256	8.86	3.488	15
22	3T	GE	Signa	256	256	1	1	1	256	8.868	3.488	15
23	3T	GE	Signa	256	256	1	1	1	256	9.148	3.624	15
24	3T	GE	Signa	256	256	1	1	1	256	11.28	4.848	20
25	3T	GE	Signa	256	256	1	1	1	256	8.836	3.488	15
26	3T	GE	Signa	256	256	1	1	1	256	9.116	3.524	15
27	3T	GE	Signa	256	256	1	1	1	256	9.128	3.624	15
28	3T	GE	Signa	256	256	1	1	1	256	9.136	3.624	15
29	3T	GE	Signa	256	256	1	1	1	256	9.148	3.624	15
30	3T	GE	Signa	256	256	1	1	1	256	9.076	3.624	15
31	3T	GE	Signa	256	256	1	1	1	256	9.128	3.624	15
32	3T	GE	Signa	256	256	1	1	1	256	9.148	3.616	15
33	3T	GE	Signa	256	256	1	1	1	256	9.12	3.624	15
34	3T	GE	Signa	256	256	1	1	1	256	9.096	3.624	15
35	3T	GE	Signa	256	256	1	1	1	256	9.048	3.616	15
36	3T	GE	Signa	256	256	1	1	1	256	9.096	3.616	15
37	3T	GE	Signa	256	256	1	1	1	256	9.096	3.616	15
38	3T	GE	Signa	256	256	1	1	1	256	9.148	3.616	15
39	3T	SIEMENS	TrioTim	256	256	1	1	1	160	1900	3.43	9
40	3T	SIEMENS	TrioTim	256	256	1	1	1	160	1900	3.43	9
41	3T	SIEMENS	TrioTim	256	256	1	1	1	160	1900	3.43	9
42	3T	SIEMENS	TrioTim	256	256	1	1	1	159	1900	3.43	9
43	3T	SIEMENS	TrioTim	256	256	1	1	1	160	1900	3.43	9

44	3T	SIEMENS	TrioTim	256	256	1	1	1	154	1900	3.43	9
45	3T	SIEMENS	TrioTim	256	256	1	1	1	160	1900	3.43	9
46	3T	SIEMENS	TrioTim	256	256	1	1	1	160	1900	3.43	9
47	3T	SIEMENS	TrioTim	256	256	1	1	1	160	1900	3.43	9
48	3T	SIEMENS	TrioTim	256	256	1	1	1	160	1900	3.43	9
49	3T	SIEMENS	TrioTim	256	256	1	1	1	160	1900	3.43	9
50	3T	SIEMENS	TrioTim	256	256	1	1	1	160	1900	3.43	9
51	3T	SIEMENS	TrioTim	256	256	1	1	1	160	1900	3.43	9
52	3T	SIEMENS	TrioTim	256	256	1	1	1	160	1900	3.43	9
53	3T	SIEMENS	TrioTim	256	256	1	1	1	160	1900	3.43	9
54	3T	SIEMENS	TrioTim	256	256	1	1	1	160	1900	3.43	9
55	3T	SIEMENS	TrioTim	256	256	1	1	1	160	1900	3.43	9
56	3T	SIEMENS	TrioTim	256	256	1	1	1	160	1900	3.43	9
57	3T	SIEMENS	TrioTim	256	256	1	1	1	160	1900	3.43	9
58	3T	SIEMENS	TrioTim	256	256	1	1	1	160	1900	3.43	9
59	3T	SIEMENS	TrioTim	256	256	1	1	1	160	1900	3.43	9
60	3T	SIEMENS	TrioTim	256	256	1	1	1	160	1900	3.43	9
61	1.5T	SIEMENS	Aera	256	256	1	1	1	160	2000	3.13	15
62	1.5T	SIEMENS	Aera	256	256	1	1	1	192	2000	3.13	15
63	1.5T	SIEMENS	Aera	256	256	1	1	1	160	2000	3.13	15
64	1.5T	SIEMENS	Aera	256	256	1	1	1	144	2000	3.13	15
65	1.5T	SIEMENS	Aera	256	256	1	1	1	160	2000	3.13	15
66	1.5T	SIEMENS	Aera	256	256	1	1	1	128	2000	3.13	15
67	1.5T	SIEMENS	Aera	256	256	1	1	1	144	2000	3.13	15
68	1.5T	SIEMENS	Aera	256	256	1	1	1	176	2000	3.13	15
69	1.5T	SIEMENS	Aera	256	256	1	1	1	176	2000	3.13	15
70	1.5T	SIEMENS	Aera	256	256	1	1	1	128	2000	3.13	15
71	1.5T	SIEMENS	Aera	256	256	1	1	1	160	2000	3.13	15
72	1.5T	SIEMENS	Aera	256	256	1	1	1	176	2000	3.13	15
73	1.5T	SIEMENS	Aera	256	256	1	1	1	128	2000	3.13	15
74	1.5T	SIEMENS	Aera	256	256	1	1	1	192	2000	3.13	15
75	1.5T	SIEMENS	Aera	256	256	1	1	1	144	2000	3.13	15
76	1.5T	SIEMENS	Aera	256	256	1	1	1	144	2000	3.13	15
77	1.5T	SIEMENS	Aera	256	256	1	1	1	144	2000	3.13	15
78	3T	SIEMENS	Verio	256	256	1	1	1	160	1900	2.93	9
79	3T	SIEMENS	Verio	256	256	1	1	1	160	1900	2.93	9
80	3T	SIEMENS	Verio	256	256	1	1	1	176	1900	2.93	9
81	3T	SIEMENS	Verio	256	256	1	1	1	160	1900	2.93	9
82	3T	SIEMENS	Verio	256	256	1	1	1	176	1900	2.93	9
83	3T	SIEMENS	Skyra	256	256	1	1	1	256	2300	2.26	8
84	3T	SIEMENS	Skyra	256	256	1	1	1	256	2300	2.26	8
85	3T	SIEMENS	Skyra	256	256	1	1	1	256	2300	2.26	8
86	3T	SIEMENS	Skyra	256	256	1	1	1	256	2300	2.26	8
87	3T	SIEMENS	Skyra	256	256	1	1	1	256	2300	2.26	8
88	3T	SIEMENS	Skyra	256	256	1	1	1	256	2300	2.26	8

Suppl. Table 2: Detailed T2*-weighted echo planar images acquisition parameters:

Subj	Mag Field	Software	Model	Matrix		Voxel Size		Slice Thickness	Slices	TR (ms)	TE (ms)	Flip Angle	Volume
1	3T	SIEMENS	Skyra	64	64	3.4375	3.4375	4.25	37	2000	25.000	78	300
2	3T	SIEMENS	Skyra	64	64	3.4375	3.4375	4.25	37	2000	25.000	78	300
3	3T	SIEMENS	Skyra	64	64	3.4375	3.4375	4.25	37	2000	25.000	78	300
4	3T	SIEMENS	Skyra	64	64	3.4375	3.4375	4.25	37	2000	25.000	78	300
5	3T	SIEMENS	Skyra	64	64	3.4375	3.4375	4.25	38	2000	25.000	78	300
6	3T	SIEMENS	Skyra	64	64	3.4375	3.4375	4.25	37	2000	25.000	78	300
7	3T	SIEMENS	Skyra	64	64	3.4375	3.4375	4.25	37	2000	25.000	78	300
8	3T	SIEMENS	Skyra	64	64	3.4375	3.4375	4.25	37	2000	25.000	78	300
9	3T	SIEMENS	Skyra	64	64	3.9063	3.9063	4.25	42	2290	25.000	78	300
10	3T	SIEMENS	Skyra	64	64	3.4375	3.4375	4.25	37	2000	25.000	78	300
11	3T	SIEMENS	Skyra	64	64	3.4375	3.4375	4.25	37	2000	25.000	78	300
12	3T	Philips	Ingenia	80	80	2.75	2.75	3.65	37	2000	25.001	78	300
13	3T	Philips	Ingenia	80	80	2.75	2.75	3.65	37	2000	25.001	78	300
14	3T	Philips	Ingenia	80	80	2.75	2.75	3.65	37	2000	25.001	78	300
15	3T	Philips	Ingenia	80	80	2.75	2.75	3.65	37	2000	25.001	78	300
16	3T	Philips	Ingenia	80	80	2.75	2.75	3.65	37	2000	25.001	78	300
17	3T	Philips	Ingenia	80	80	2.75	2.75	3.65	37	2000	25.001	78	300
18	3T	GE	Signa	64	64	3.75	3.75	3.70	40	2000	25.000	90	300
19	3T	GE	Signa	64	64	3.4375	3.4375	3.70	40	2000	25.000	90	300
20	3T	GE	Signa	64	64	3.4375	3.4375	3.70	40	2000	25.000	90	300
21	3T	GE	Signa	64	64	3.75	3.75	3.70	40	2100	25.000	90	300
22	3T	GE	Signa	64	64	3.4375	3.4375	3.70	40	2000	25.000	90	300
23	3T	GE	Signa	64	64	3.75	3.75	3.70	40	2000	25.000	90	300
24	3T	GE	Signa	64	64	3.4375	3.4375	3.70	38	2000	25.000	78	300
25	3T	GE	Signa	64	64	3.4375	3.4375	3.70	44	2200	25.000	78	300
26	3T	GE	Signa	64	64	3.4375	3.4375	3.70	46	2300	25.000	78	300
27	3T	GE	Signa	64	64	3.4375	3.4375	3.70	39	2000	25.000	78	300
28	3T	GE	Signa	64	64	3.4375	3.4375	3.70	40	2000	25.000	78	300
29	3T	GE	Signa	64	64	3.4375	3.4375	3.70	42	2100	25.000	78	300
30	3T	GE	Signa	64	64	3.4375	3.4375	3.70	42	2138	25.000	78	300
31	3T	GE	Signa	64	64	3.4375	3.4375	3.70	45	2297	25.000	78	300
32	3T	GE	Signa	64	64	3.4375	3.4375	3.70	40	2000	25.000	78	300
33	3T	GE	Signa	64	64	3.4375	3.4375	3.70	43	2150	25.000	78	300
34	3T	GE	Signa	64	64	3.4375	3.4375	3.70	40	2000	25.000	78	300
35	3T	GE	Signa	64	64	3.4375	3.4375	3.70	40	2113	25.000	78	300
36	3T	GE	Signa	64	64	3.4375	3.4375	3.70	40	2000	25.000	78	300
37	3T	GE	Signa	64	64	3.4375	3.4375	3.70	40	2000	25.000	78	300
38	3T	GE	Signa	64	64	3.4375	3.4375	3.70	44	2200	25.000	78	300
39	3T	SIEMENS	TrioTim	64	64	3.4375	3.4375	4.25	37	2000	25.000	90	300
40	3T	SIEMENS	TrioTim	64	64	3.4375	3.4375	4.25	37	2000	25.000	90	300
41	3T	SIEMENS	TrioTim	64	64	3.4375	3.4375	4.25	37	2000	25.000	90	300
42	3T	SIEMENS	TrioTim	64	64	3.4375	3.4375	4.25	37	2000	25.000	90	300
43	3T	SIEMENS	TrioTim	64	64	3.4375	3.4375	4.25	37	2000	25.000	90	300

44	3T	SIEMENS	TrioTim	64	64	3.4375	3.4375	4.25	37	2000	25.000	90	300
45	3T	SIEMENS	TrioTim	64	64	3.4375	3.4375	4.25	37	2000	25.000	90	300
46	3T	SIEMENS	TrioTim	64	64	3.4375	3.4375	4.25	37	2000	25.000	90	300
47	3T	SIEMENS	TrioTim	64	64	3.4375	3.4375	4.25	37	2000	25.000	90	300
48	3T	SIEMENS	TrioTim	64	64	3.4375	3.4375	4.25	37	2000	25.000	90	300
49	3T	SIEMENS	TrioTim	64	64	3.4375	3.4375	4.25	37	2000	25.000	90	300
50	3T	SIEMENS	TrioTim	64	64	3.4375	3.4375	4.25	37	2000	25.000	90	300
51	3T	SIEMENS	TrioTim	64	64	3.4375	3.4375	4.25	37	2000	25.000	90	300
52	3T	SIEMENS	TrioTim	64	64	3.4375	3.4375	4.25	37	2000	25.000	78	300
53	3T	SIEMENS	TrioTim	64	64	3.4375	3.4375	4.25	37	2000	25.000	78	300
54	3T	SIEMENS	TrioTim	64	64	3.4375	3.4375	4.25	37	2000	25.000	78	300
55	3T	SIEMENS	TrioTim	64	64	3.4375	3.4375	4.25	37	2000	25.000	78	300
56	3T	SIEMENS	TrioTim	64	64	3.4375	3.4375	4.25	37	2000	25.000	78	300
57	3T	SIEMENS	TrioTim	64	64	3.4375	3.4375	4.25	37	2000	25.000	78	300
58	3T	SIEMENS	TrioTim	64	64	3.4375	3.4375	4.25	37	2000	25.000	78	300
59	3T	SIEMENS	TrioTim	64	64	3.4375	3.4375	4.25	37	2000	25.000	78	300
60	3T	SIEMENS	TrioTim	64	64	3.4375	3.4375	4.25	37	2000	25.000	78	300
61	1.5T	SIEMENS	Aera	64	64	3.4375	3.4375	4.48	34	2000	25.000	78	300
62	1.5T	SIEMENS	Aera	64	64	3.4375	3.4375	4.48	34	2000	25.000	78	300
63	1.5T	SIEMENS	Aera	64	64	3.75	3.75	4.48	34	2000	25.000	78	300
64	1.5T	SIEMENS	Aera	64	64	3.4375	3.4375	4.48	34	2070	25.000	78	300
65	1.5T	SIEMENS	Aera	64	64	3.4375	3.4375	3.81	41	2500	25.000	78	300
66	1.5T	SIEMENS	Aera	64	64	3.4375	3.4375	3.81	34	2000	25.000	78	300
67	1.5T	SIEMENS	Aera	64	64	3.4375	3.4375	3.81	34	2000	25.000	78	300
68	1.5T	SIEMENS	Aera	64	64	3.4375	3.4375	3.81	34	2000	25.000	78	300
69	1.5T	SIEMENS	Aera	64	64	3.4375	3.4375	3.81	41	2370	25.000	78	300
70	1.5T	SIEMENS	Aera	64	64	3.4375	3.4375	3.81	34	2000	25.000	78	300
71	1.5T	SIEMENS	Aera	64	64	3.4375	3.4375	3.81	34	2000	25.000	78	300
72	1.5T	SIEMENS	Aera	64	64	3.5938	3.5938	3.81	38	2200	25.000	78	300
73	1.5T	SIEMENS	Aera	64	64	3.4375	3.4375	3.81	34	2000	25.000	78	300
74	1.5T	SIEMENS	Aera	64	64	3.4375	3.4375	3.81	45	2600	25.000	78	300
75	1.5T	SIEMENS	Aera	64	64	3.4375	3.4375	3.81	37	2140	25.000	78	300
76	1.5T	SIEMENS	Aera	64	64	3.4375	3.4375	3.81	34	2000	25.000	78	300
77	1.5T	SIEMENS	Aera	64	64	3.4375	3.4375	3.81	34	2000	25.000	78	300
78	3T	SIEMENS	Verio	64	64	3.4375	3.4375	3.91	36	2000	25.000	78	300
79	3T	SIEMENS	Verio	64	64	3.4375	3.4375	3.91	34	2000	25.000	78	300
80	3T	SIEMENS	Verio	64	64	3.4375	3.4375	3.91	34	2000	25.000	78	300
81	3T	SIEMENS	Verio	64	64	3.4375	3.4375	3.91	34	2000	25.000	78	300
82	3T	SIEMENS	Verio	64	64	3.4375	3.4375	3.91	40	2000	25.000	78	300
83	3T	SIEMENS	Skyra	64	64	3.4375	3.4375	4.25	37	2000	25.000	78	300
84	3T	SIEMENS	Skyra	64	64	3.4375	3.4375	4.25	37	2000	25.000	78	300
85	3T	SIEMENS	Skyra	64	64	3.4375	3.4375	4.25	37	2000	25.000	78	300
86	3T	SIEMENS	Skyra	64	64	3.4375	3.4375	4.25	37	2000	25.000	78	300
87	3T	SIEMENS	Skyra	64	64	3.4375	3.4375	4.25	37	2000	25.000	78	300
88	3T	SIEMENS	Skyra	64	64	3.4375	3.4375	4.25	37	2000	25.000	78	300

Suppl. Table 3: Denoising pipelines and the total number of regressors used in each of them.

Denoising Pipeline	**nr. of regressors**
6HMP	6
24HMP + 2Phys	26
24HMP + 2Phys + GSR	27
24HMP + aCompCor	34
24HMP + aCompCor + GSR	35
24HMP + aCompCor50	24 + *k*
24HMP + aCompCor50 + GSR	25 + *k*
2Phys + ICA-AROMA	2 + *k*
2Phys + ICA-AROMA + GSR	3 + *k*
24HMP + 2Phys + SpikeReg	26 + *k*
24HMP + 2Phys + SpikeReg + GSR	27 + *k*
24HMP + 2Phys + Scrubbing	26 + *k*
24HMP + 2Phys + Scrubbing + GSR	27 + *k*
6HMP + aCompCor + SpikeReg	16 + *k*
6HMP + aCompCor + SpikeReg + GSR	17 + *k*
24HMP + aCompCor + SpikeReg	34 + *k*
24HMP + aCompCor +SpikeReg + GSR	35 + *k*

Abbreviations: HMP = Head Motion Parameters; Phys = physiological regressors (white matter (WM) and cerebrospinal fluid (CSF) average time-series); GSR = Global Signal Regression; aCompCor = anatomical Component Correction; SpikeReg = Spike regression.
k = variable that represents the number of additional regressors estimated by the denoising method, which varies from subject to subject. For aCompCor50, *k* is the number of components that explain 50% of the variance in each WM and CSF compartments; for ICA-AROMA, *k* represents the total number of components classified as noise; for SpikeReg and Scrubbing, *k* represents the number of contaminated volumes. Ideally, good denoising pipelines should use fewer regressors in the model, losing fewer degrees of freedom.

Suppl. Table 4: EpiBioS4Rx's Principal Investigators and affiliated institutions.

Principal Investigator/Author	Affiliated Institutions
Alaa Kamnaksh	Uniformed Services University, United States
Alicia Au	University of Pittsburgh, United States
Andrew Morokoff	Royal Melbourne Hospital, United States
Arthur Toga	University of Southern California, United States
Ben Ellingson	David Geffen School of Medicine at UCLA, United States
Brandon Foreman	University of Cincinnati, United States
Courtney L. Robertson	Johns Hopkins University, United States
Courtney Real	David Geffen School of Medicine at UCLA, United States
David McArthur	David Geffen School of Medicine at UCLA, United States
Denes Agoston	Uniformed Services University, United States
Elisa Yam	David Geffen School of Medicine at UCLA, United States
Emily J. Gilmore	Yale University, United States
Eric Rosenthal	Harvard University/Massachusetts General Hospital, United States
Jan Claassen	Columbia University, United States
Lara Zimmermann	University of California, Davis, United States
Lawrence Hirsch	Yale University, United States
Manuel Buitrago Blanco	David Geffen School of Medicine at UCLA, United States
Michael J. Bell	Children's National Health System, United States
Ramon Diaz-Arrastia	University of Pennsylvania, United States
Richard Staba	David Geffen School of Medicine at UCLA, United States
Susana Martinez	David Geffen School of Medicine at UCLA, United States
Terrence O'Brien	Royal Melbourne Hospital, United States
Dominique Duncan	University of Southern California, United States
Frederick A. Willyerd	Phoenix Children's Hospital, United States
Jerome Engel Jr.	David Geffen School of Medicine at UCLA, United States
Kristine O'Phelan	University of Miami, United States
Martin Hunn	The Alfred Hospital Melbourne, Australia
Nicholas Abend	University of Pennsylvania, United States
Thomas P. Bleck	Rush University, United States
Vikesh Shrestha	David Geffen School of Medicine at UCLA, United States

a

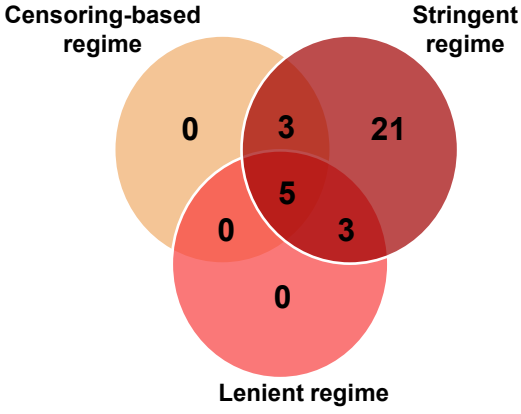
Censoring-based regime
Stringent regime
Lenient regime
0
3
21
5
0
3
0

b

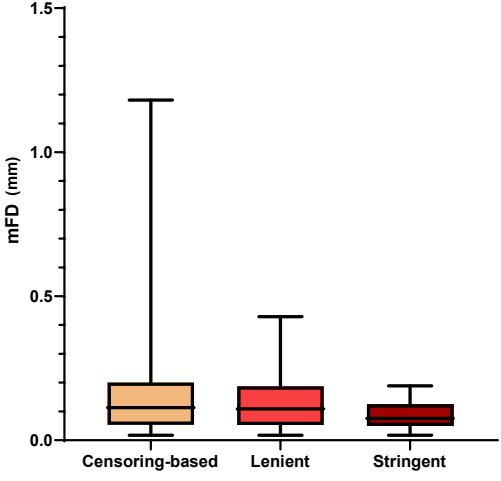
mFD (mm)
1.5
1.0
0.5
0.0
Censoring-based
Lenient
Stringent

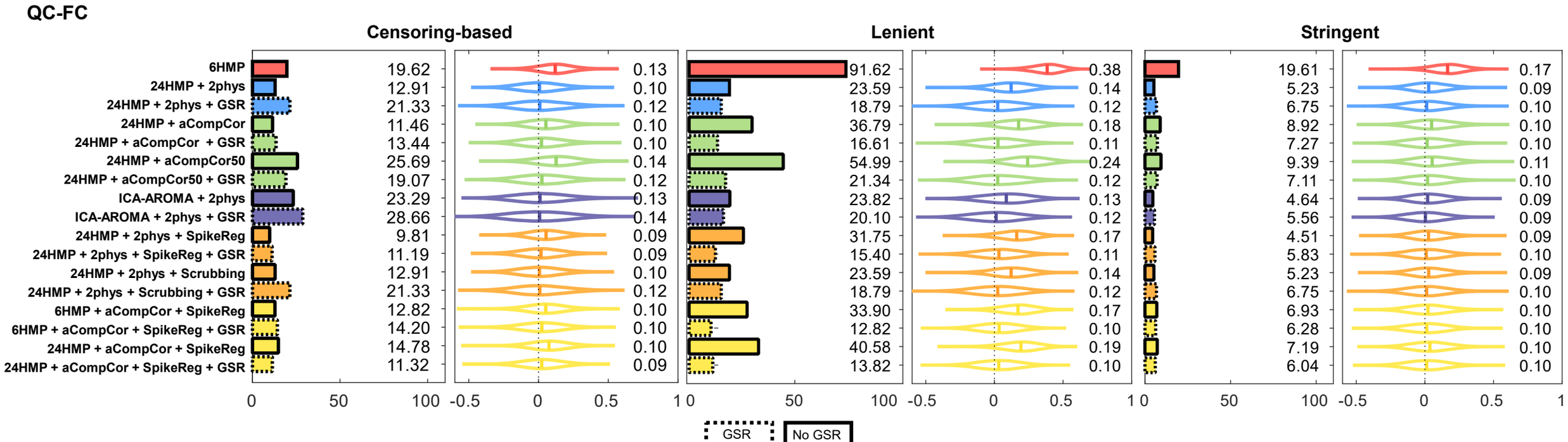
QC-FC
Censoring-based
Lenient
Stringent
6HMP
24HMP + 2phys
24HMP + 2phys + GSR
24HMP + aCompCor
24HMP + aCompCor + GSR
24HMP + aCompCor50
24HMP + aCompCor50 + GSR
ICA-AROMA + 2phys
ICA-AROMA + 2phys + GSR
24HMP + 2phys + SpikeReg
24HMP + 2phys + SpikeReg + GSR
24HMP + 2phys + Scrubbing
24HMP + 2phys + Scrubbing + GSR
6HMP + aCompCor + SpikeReg
6HMP + aCompCor + SpikeReg + GSR
24HMP + aCompCor + SpikeReg
24HMP + aCompCor + SpikeReg + GSR
19.62
12.91
21.33
11.46
13.44
25.69
19.07
23.29
28.66
9.81
11.19
12.91
21.33
12.82
14.20
14.78
11.32
0.13
0.10
0.12
0.10
0.10
0.14
0.12
0.13
0.14
0.09
0.09
0.10
0.12
0.10
0.10
0.10
0.09
91.62
23.59
18.79
36.79
16.61
54.99
21.34
23.82
20.10
31.75
15.40
23.59
18.79
33.90
12.82
40.58
13.82
0.38
0.14
0.12
0.18
0.11
0.24
0.12
0.13
0.12
0.17
0.11
0.14
0.12
0.17
0.10
0.19
0.10
19.61
5.23
6.75
8.92
7.27
9.39
7.11
4.64
5.56
4.51
5.83
5.23
6.75
6.93
6.28
7.19
6.04
0.17
0.09
0.10
0.10
0.10
0.11
0.10
0.09
0.09
0.09
0.10
0.09
0.10
0.10
0.10
0.10
0.10
0
50
100
-0.5
0
0.5
1
GSR
No GSR

QC-FC Distance dependence

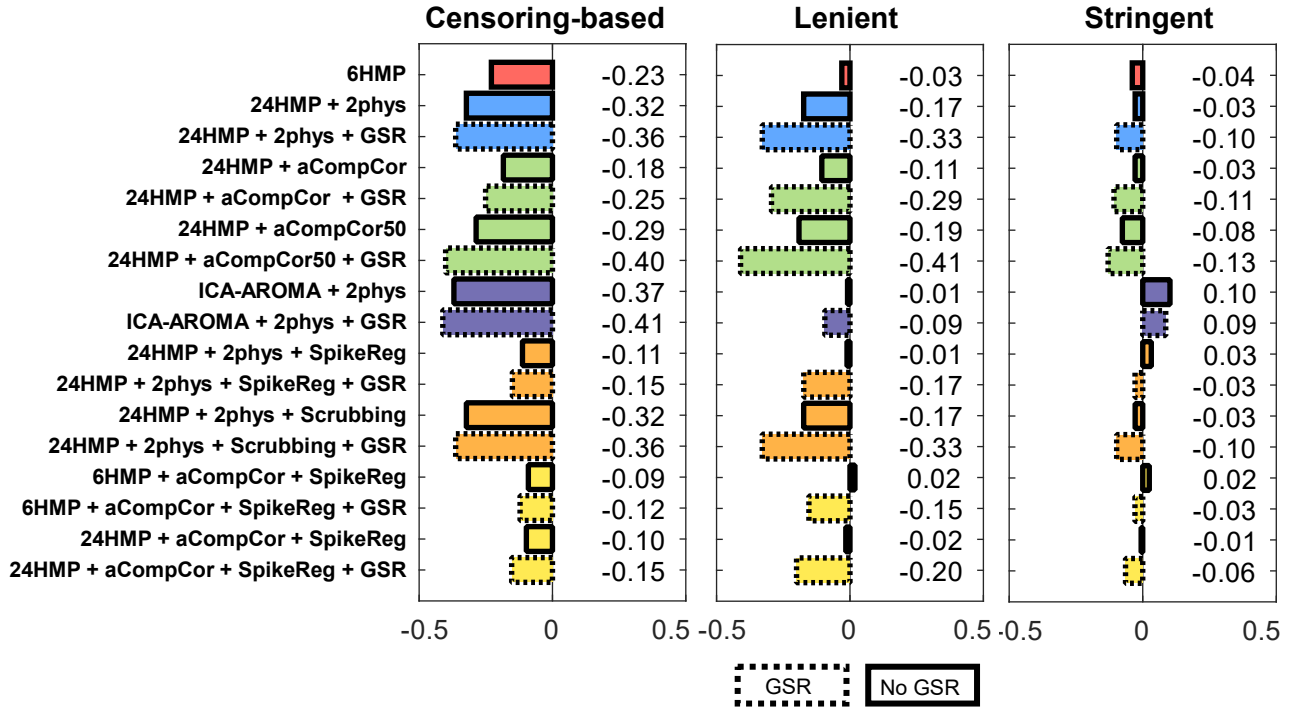

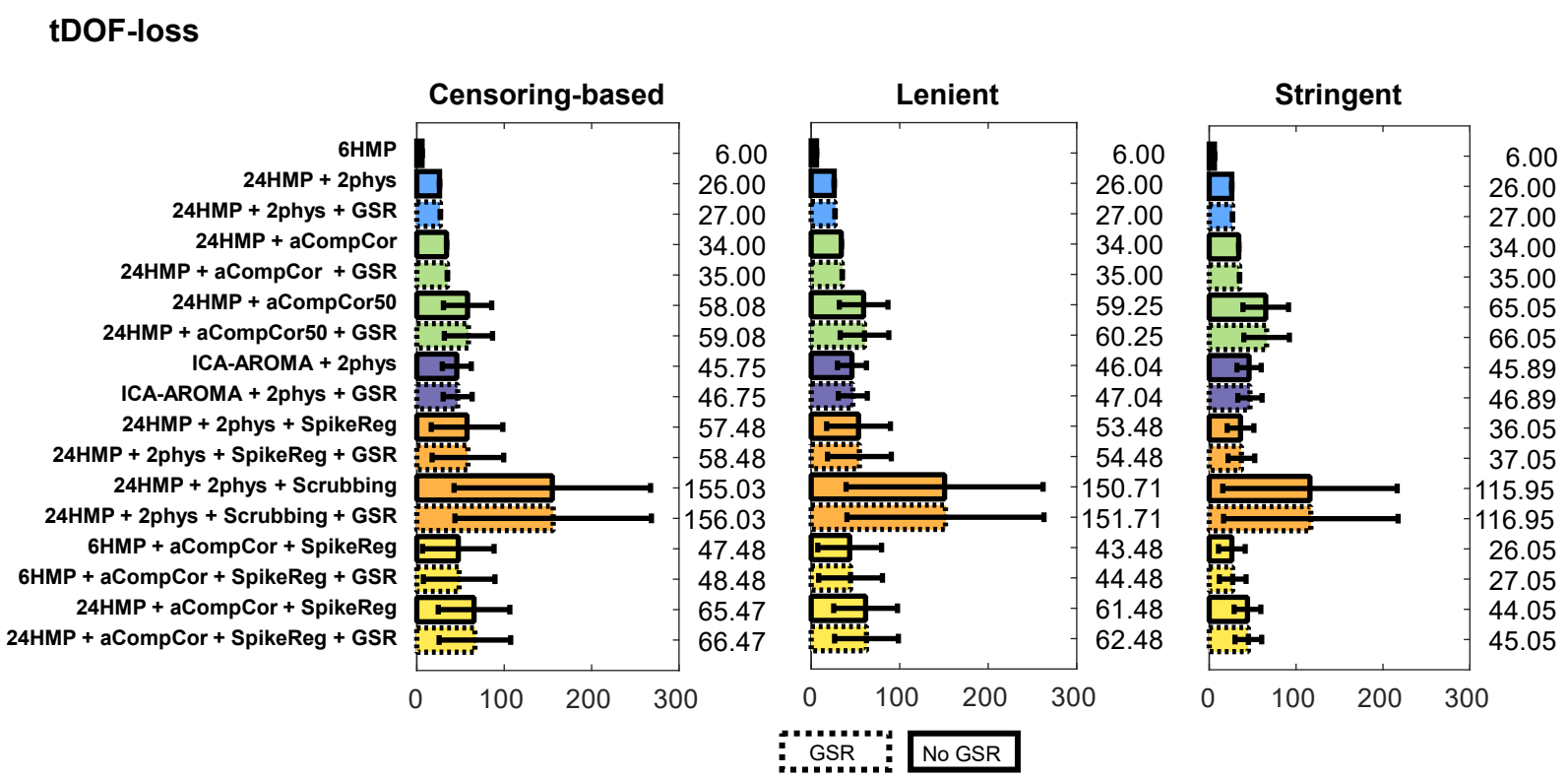
tDOF-loss
Censoring-based
Lenient
Stringent
6HMP
24HMP + 2phys
24HMP + 2phys + GSR
24HMP + aCompCor
24HMP + aCompCor + GSR
24HMP + aCompCor50
24HMP + aCompCor50 + GSR
ICA-AROMA + 2phys
ICA-AROMA + 2phys + GSR
24HMP + 2phys + SpikeReg
24HMP + 2phys + SpikeReg + GSR
24HMP + 2phys + Scrubbing
24HMP + 2phys + Scrubbing + GSR
6HMP + aCompCor + SpikeReg
6HMP + aCompCor + SpikeReg + GSR
24HMP + aCompCor + SpikeReg
24HMP + aCompCor + SpikeReg + GSR
6.00
26.00
27.00
34.00
35.00
58.08
59.08
45.75
46.75
57.48
58.48
155.03
156.03
47.48
48.48
65.47
66.47
6.00
26.00
27.00
34.00
35.00
59.25
60.25
46.04
47.04
53.48
54.48
150.71
151.71
43.48
44.48
61.48
62.48
6.00
26.00
27.00
34.00
35.00
65.05
66.05
45.89
46.89
36.05
37.05
115.95
116.95
26.05
27.05
44.05
45.05
0
100
200
300
GSR
No GSR